Atmos. Chem. Phys. Discuss., 8, 13159–13195, 2008
www.atmos-chem-phys-discuss.net/8/13159/2008/

Atmospheric Chemistry and Physics Discussions

Regional-scale modeling of near-ground ozone in the Central East China, source attributions and an assessment of outflow to East Asia – The role of regional-scale transport during MTX2006

J. Li[1,2], Z. Wang[2], H. Akimoto[1], K. Yamaji[1], M. Takigawa[1], P. Pochanart[1], Y. Liu[1], and Y. Kanaya[1]

[1]Frontier Research Center for Global Change, Japan Agency for Marine-Earth Science and Technology, Japan
[2]State Key Laboratory of Atmospheric Boundary Layer Physics and Atmospheric Chemistry(LAPC), Nansen-Zhu International Research Center (NZC), Institute of Atmospheric Physics, Chinese Academy of Sciences, Beijing, People's Republic of China

Received: 7 April 2008 – Accepted: 17 June 2008 – Published: 10 July 2008

Correspondence to: J. Li (lijie8074@jamstec.go.jp)

Published by Copernicus Publications on behalf of the European Geosciences Union.

Abstract

A 3-D regional chemical transport model, the Nested Air Quality Prediction Model System (NAQPMS), with an on-line tracer tagging module was applied to study the source of the near-ground (<1.5 km above ground level) ozone at Mt. Tai (36.25°N, 117.10°E, 1534 m a.s.l.) in Central East China (CEC) during the Mount Tai eXperiment 2006 (MTX2006): regional ozone photochemistry and aerosol studies in Central East China in June, 2006. The model reproduced the temporal and spatial variations of near-ground ozone and other pollutants. In particular, the model captured highly polluted and clean cases well. The simulated near-ground ozone over CEC is 60–85 ppbv (parts per billion by volume), higher than those (20–50 ppbv) in Japan and over the North Pacific. The simulated tagged tracer indicates that the regional-scale transport of chemically produced ozone over other areas in CEC contributes to the most fractions (49%) of the near-ground mean ozone at Mt. Tai in June, rather than the in-situ photochemistry (12%). Due to high anthropogenic and biomass burning emissions, the contributions of the ground ozone from the southern part of CEC plays the most important role (32.4 ppbv, 37.9% of total ozone) in the monthly mean ozone concentration at Mt. Tai, which even reached 59 ppbv (62%) on 6–7 June 2006. The monthly mean horizontal distribution of chemically produced ozone from various source regions indicates that the spatial distribution of O_3 over CEC is controlled by the photochemical reactions. In addition, the regional-scale transport of pollutants also plays an important role in the spatial and temporal distribution of ozone over CEC. The chemically produced ozone from the southern part of the study region can be transported northeastwardly to the northern rim of CEC. The mean contribution is 5–10 ppbv, and it can reach 25 ppbv during high ozone events. This work also studied the outflow of CEC ozone and its precursors, as well as their influences and contributions to the ozone level over adjacent regions/countries. It shows that the contribution of CEC ozone to mean ozone mixing ratios over Korea Peninsula and Japan is 5–15 ppbv, of which about half was due to the direct transport of ozone from CEC and half was contributed by the ozone produced

ACPD

8, 13159–13195, 2008

locally by the transported ozone precursors from CEC.

1 Introduction

The importance of tropospheric ozone (O_3) in air quality, atmospheric chemistry and climate change has been recognized over the past decades (IPCC, 2001; Brasseur et al., 1999). Apart from the downward injection of stratospheric ozone, photochemical reactions involving oxides of nitrogen (NO_x=NO+NO_2), carbon monoxide (CO), methane (CH_4) and volatile organic compounds (VOCs), also plays a key role in ozone production, especially in industrialized regions (Crutzen et al., 1999).

Along with the rapid urbanization and industrialization processes, the emissions of O_3 precursors have significantly increased in China in contrast to a significant decrease in Europe and little change in North America and Japan (Naja and Akimoto, 2004; Streets and Waldhoff, 2000). As the biggest emitters of anthropogenic trace gas and aerosols in China (NO_x emissions reached 3600 Gg/a in 2000, 32% of the total emissions in China) (Streets and Waldhoff, 2000), the Central East China (CEC, 30°N–40°N, 110°E-130°E, Sect. 2.2) shows a continuous and marked increase in tropospheric NO_2 column densities during 1996–2004 (Richter et al., 2005; Akimoto et al., 2006). Consequently, serious regional-scale near-ground high ozone level has been recorded in this region in early summer, rather than spring (Ding et al., 2008; Li et al., 2007). From our observations at three mountain sites (Mt. Tai, Hua and Huang), located in the middle, west and south of CEC, the maximum monthly ozone concentration of above 60 ppbv in May–June, with a maximum hourly ozone level above 150 ppbv, have been found (Pochanart, personal communication; Li et al., 2007). Observations at Shangdianzi (a rural site in northern CEC) showed that averaged maximum hourly ozone in June exceeds 120 ppbv (Liu et al, 2006). During a 39-day observation in a rural area located north of Beijing in June–July 2005, Wang et al found that there were 13 days with 1-h O_3 mixing ratio exceeded 120 ppbv and a maximum level of 286 ppbv, which is the highest reported value in open literatures in China (Wang, et al., 2006a). High ozone levels

ACPD
8, 13159–13195, 2008

have also been frequently reported of another rural site, Lin'an (a rural site in southern CEC) (Wang et al., 2001a; Cheung et al., 2001; Xu et al., 2008). Gao et al. (2005) reported that monthly mean ozone of local air masses over CEC was above 60 ppbv in July. Modeling studies further support the above mentioned facts and demonstrate that CEC has the most net chemical production over East Asia in summer (Zhu et al., 2004; Yamaji et al., 2006; Li et al., 2007).

Regional-scale transport of pollutants was considered to play an important role in the regional high O_3 level over CEC. Satellite-measured tropospheric NO_2column densities show an increase rate of 27.5% in the southeast part of CEC during 2000–2005, higher than other parts of the study region (He et al., 2007). Observations show that the transport of Beijing plumes superimposed on pollution contributed by regional sources is the dominating mechanism of high ozone at a rural site in northern CEC in June-July (Wang et al., 2006a). Wang et al. (2006b) and Li et al. (2007) also found that regional-scale transport contributes not only to high ozone levels in certain events, but also to monthly mean ozone concentration. The inter-continental transport of ozone from this region in summer has also been reported in some recent work (Pochanart et al., 2004; Zhu et al., 2004). As a matter of fact, to better understand the sources and transport of regional high ozone level in CEC, also to reduce the possibility of the occurrence of future high ozone events, a systematic research at a representative site over CEC and quantitatively evaluation the contributions of regional-scale transport from various source regions in "regional" context, rather than individual source, was performed.

To study ozone chemistry/transport and aerosol composition/chemistry/transport over CEC, the Frontier Research Center for Global Change (FRCGC), the Japan Agency for Marine-Earth Science and Technology (JAMSTEC) and the Institute of Atmospheric Physics (IAP), Chinese Academy of Sciences (CAS) conducted a filed campaign – the Mount Tai eXperiment 2006 (MTX2006): regional ozone photochemistry and aerosol studies in Central East China at Mt. Tai (36.25°N, 117.10°E , 1534 m a.s.l., an isolated single mountain in the middle of CEC) in June 2006, when the highest monthly mean ozone occurred. Measurements were taken for the concentration of

surface O_3, CO, NO_x, VOCs, element carbon (EC), organic carbon (OC), chemical compositions of aerosols and J-values. Tropospheric NO_2 column and meteorological variables are also measured. Details associated with the procedures of conducting this experiment, the sampling instruments, and the evolution of the composition of trace gases can be found in Akimoto et al. (this issue) and Kanaya et al. (this issue).

The main objective of this paper is to investigate the source regions of high ozone over CEC. The focus is to quantitatively evaluate the contributions of regional-scale transport from various source regions to the accumulation and distribution of ozone over CEC in a "regional" context and the transport of ozone from China to East Asia by using an Eulerian regional chemical model, the Nested Air Quality Prediction Modeling System (NAQPMS), with an on-line tracer tagging module. This study also provides us with a prototype of how to analyze model uncertainties. A brief description of the regional chemical transport model and the on-line tagged-tracer approach were presented first, followed by the evaluation of the model by comparing simulations with observations in the MTX2006 field campaign. Then the contributions from various source regions are quantitatively evaluated. At last, contributions of the near-ground ozone in CEC to East Asia are discussed.

This paper appears to be the first attempt to quantitatively provide a perspective about the impacts of ozone from various source regions within CEC. It is also expected to provide valuable insights for policy makers to help decrease the ozone level in this region.

2 Model description

To differentiate the contributions from various source regions over CEC, we apply a tagged tracer method developed by Wang et al. (in preparation) in the framework of NAQPMS. Compared with the classic sensitive analysis with turning on/off targeted source regions, the tagged tracer method provides a different and more efficient measurement of relative importance of various source regions without the errors due to

ACPD
8, 13159–13195, 2008

the important nonlinearities in the transport and fast photochemistry of ozone and its precursors. Similar studies can also be found in other works (Wang et al., 1998; Sudo and Akimoto, 2007). Details on the model and the tagged tracer module are described in the following subsections.

2.1 Regional chemical transport model

A detailed description of NAQPMS used in this study can be found in previous works (Wang et al., 1996, 2000, 2001b, 2006b; Li et al., 2007). The following is a brief summary to facilitate the discussions below. NAQPMS is implemented in two steps: a mesoscale meteorological model to generate the wind field and a nested chemical transport module. The meteorological model is a three-dimensional, non-hydrostatic mesoscale modeling system, which is called the fifth generation Mesoscale Model (MM5) developed by the Penn State University (PSU) and the National Center for Atmospheric Research (NCAR) (Grell et al., 1994). The initial and boundary conditions for MM5 are from NCAR/NCEP $1^{\circ}\times1^{\circ}$ reanalysis data sets at 6-h intervals. The nested chemical transport module includes advection/convection and diffusion processes, gas/aqueous chemistry, parameterization of dry/wet deposition and a unique dust particle deflation module (Wang et al, 2000, 2002; Zhu et al., 2004). The Carbon-Bond Mechanism Z (CBM-Z), which is composed of 133 reactions for 53 species, was applied. Compared with Carbon-Bond IV, the CBM-Z extends the framework to function properly at larger spatial and longer time scales (Zaveri and Peters, 1999). The advection scheme employs a simplified but accurate mass conservative peak-preserving, mixing ratio bounded advection algorithm (Walcek and Aleksic, 1998). Dry deposition module is updated to the Wesely's scheme (1989). Since 1995, NAQPMS has been successfully used to model dust events (Wang et al., 2000), the transport and chemical processes of pollutants (Sulfur, O_3) (Li et al., 2007; Wang et al., 2000, 2006b; Zhu et al., 2004), and the interactions between mineral aerosols and acid rain over East Asia (Wang et al., 2002).

In this study, the model domain of NAQPMS simulation shown in Fig. 1 is composed

ACPD
8, 13159–13195, 2008

of two nested domains. The coarser domain is 6075×4620 km^2 on a Lambert conformal map projection with 81 km grid resolution. The nested domain is divided into 72×69 horizontal grids with 27 km resolution, as Mt. Tai sits in the center of the inner domain. Vertically, the model uses ten layers in terrain following coordinate, with five layers within the lowest one kilometer above the surface. Vertical-grid spacing is increased gradually from 50 m at the surface to 2000 m at the top (10 km a.s.l.).

The anthropogenic emission inventory (fossil fuels, biofuels, and industrial emissions excluding biomass burning, the same below) used in this study was derived from the bottom-up Regional Emission inventory in ASia (REAS) with 0.5°×0.5° resolution in 2006, which was based on several energy statistics, emission factors and economical information (Ohara et al., 2007). Much more detailed information on the emission inventory can be found in the paper of Yamaji (this issue). In this work, REAS emissions are mapped into 0.1°×0.1° grid by using the distribution of Streets's inventory (personal communication) with 0.1° resolution. Biomass burning emission inventory of China is based on the work of Cao et al. (2005), who provided a provincial resolution inventory of China including SO_2, NO_x, CH_4, CO, BC, OC and VOCs. Biomass burning emissions are projected into 1°×1° grid based on the Global Fire Emissions Database version 2 (GFEDv2) (van der Werf et al., 2006) resampled to an 8-day time step using MODIS fire hot spots (Giglio et al., 2003) with 1°×1° resolution by calculating the relative fractions of emissions on every grid in one province in GFEDv2. The emissions of countries other than China are directly from GFEDv2. Biogenic hydrocarbon emissions are from the Global Emissions Inventory Activity (GEIA) (Guenther et al., 1995).

The simulation started at 08:00 UTC on 1 May 2006 and run through the end of June 2006. The first 14 days are regarded as the spin-up period to reduce the influence of initial conditions. The initial and boundary conditions (lateral and top) of several chemical species (O_3, CO, NO_x, ethane and propane) are provided by the 3-hourly outputs from a coupled tropospheric chemistry climate model CHASER (Sudo et al., 2002) with 2.8°×2.8° horizontal resolution.

ACPD
8, 13159–13195, 2008

2.2 Tracer tagging

O_3 was labeled by the geographical location in which region it was formed. O_3 from the top and lateral boundary and initial conditions are also labeled. The fraction of any tagged ozone ($O_3{}^T$) in total ozone is calculated at a 5-min time step, the same as the total ozone. We assume that different phases of $O_3{}^T$ are mixed well in each grid, and each $O_3{}^T$ shares the same loss coefficients as total ozone (including outflow, chemical destruction, and dry and wet removals), so all of the removal processes have no alteration on the fraction of each $O_3{}^T$ in the total ozone in any grid. The tendency of any $O_3{}^T$ fraction in any grid can be described as follows:

$$\left(\frac{dF_{O_3{}^T}}{dt}\right)_{ij} = \left(P_{ij} + (M_{ij})_{\text{dif+adv+conv}}\right)/O_3 \quad (1)$$

where i and j represent the ith geographical source region and the jth grid. $F_{O_3{}^T}$ represents the fraction of the ith $O_3{}^T$ in jth grid. P_{ij} is the gross photochemical ozone production of the ith source region in the jth grid. Here, if the jth grid is within the tagged geographical source region i, P_{ij} is calculated as described in the previous work (Davis et al., 2003; Kondo et al., 2004). Otherwise, P_{ij} is equal to zero (outside the region i). $(M_i)_{\text{dif+adv+conv}}$ is the $O_3{}^T$ inflow from the adjacent grids due to advection, diffusion, and convection, and calculated by the inflow fluxes and the ith $O_3{}^T$ fraction in those adjacent grids. O_3 is the mixing ratio of total ozone.

This study tagged 20 source regions in East Asia. Lateral and top boundary and initial ozone are also tagged. The location and description of each region are indicated in Fig. 1 and Table 1. Here, CEC consists of Local, SSD, ESD, NSD, HBT, SX, HN, AH, JS and CHNSEA as shown in Fig. 1. Local refers to Tai'an and Laiwu city, a region with 1×10^5 km^2 area and 6.6 million people. Mt. Tai is located in this region. SSD, ESD and NSD are the Southern, Eastern and Northern parts of ShanDong province, respectively. HBT includes Hebei province, Beijing and Tianjin city, where steel indus-

ACPD
8, 13159–13195, 2008

try, traffic are the major emitters in China. SX represents ShanXi province, and it is the biggest coal producer in China (248.9 million tons, 25% of the country's total). HN (HeNan province) boasts the largest population in China (97.7 million). AH and JS represent AnHui and JiangSu province, which have the most developed petrochemistry industry in China. CHNSEA includes the Bohai Sea, the Huanghai Sea and the East China Sea, which are all close enough to CEC and was considered to influence the outflow of CEC ozone precursors which could further affect the ozone mixing ratios.

The monthly NO_x emissions of the ten regions within CEC are presented in Table 2. Biomass burning emissions with 8-day time step are also shown for its high temporal variability. Table 2 shows that biomass burning contributes comparable NO_x emissions with anthropogenic activities in the southern parts of CEC, especially during the first 16 days of June. This exerts influence on the ozone level in CEC.

3 Results and discussions

3.1 Model evaluation

3.1.1 Observed ozone and related species at Mt. Tai

Figure 2 presents the time series of hourly averaged concentration of O_3, CO, NO_x and BC at Mt. Tai. The air quality at Mt. Tai during the campaign period was not good. Over the 30 days, there were 14 days with the highest ozone mixing ratio exceed the China's air quality standard for ozone with hourly value of 100 ppbv (Grade II). The observed mean O_3 of 82 ppbv is not only 30 ppbv higher than observations at the rural/remote sites over the North Pacific (Pochanart et al., 2004), but also higher than the previous modeled results for this particular location (Yamaji et al., 2006, http://www.atmos.washington.edu/~jaegle/geoso3_start.html). The mean concentrations of CO and BC reached 560 ppbv and 3.4 μgC/m^3, both of which are higher than the satellite observations (http://mopitt.eos.ucar.edu/mopitt/data/plots/mapsv3_mon.html).

ACPD
8, 13159–13195, 2008

In this study, two high pollution episodes are defined: 16:00 UTC on 5 June–16:00 UTC on 7 June (Case I) and 04:00 UTC on 11 June–11:00 UTC on 13 June (Case II). The mean concentrations of O_3, CO, NO_x and BC in Case II reached up to 95 ppbv, 700 ppbv, 2.5 ppbv and 8 μgC/m^3, with maximums of 160 ppbv, 1700 ppbv, 8 ppbv and 20 μgC/m^3, respectively. In the following sections, we will study the source regions and transport of high ozone, focusing on those two cases. Furthermore, to better understand the sources of the high level pollutants, we select the 16:00 UTC on 08 June–23:00 UTC on 10 June (Case III) as the reprehensive clear case, when the concentration of O_3, CO, NO_x and BC are 64 ppbv, 276 ppbv, 1.3 ppbv and 1.3 μgC/m^3.

3.1.2 Comparison with observations in the study period

Figure 3a shows the time variations of the predicted and observed hourly averaged meteorological and chemical variables at Mt. Tai. The model is able to reproduce the synoptic features of the meteorological variables, especially the change of the wind direction from northward to southward during the two heavy pollution episodes. The simulated time series of ozone concentration is globally satisfactory as the model effectively reproduced the daily variations. The correlation coefficients of hourly and daily ozone concentrations between the modeled and observed values are 0.56 and 0.69 (Table 3). The simulated monthly mean ozone (85 ppbv) shows that the model captures the same magnitude as observations, which is confirmed by the small Mean Bias (MB) and the Root Mean Square Error (RMSE) of hourly and daily mean ozone concentration (Table 3). NO_x concentrations are also well reproduced by the model. The simulated correlation, NB and RMSE of daily mean NO_x is 0.62, 0.1 ppbv and 0.50 ppbv, respectively. A general agreement can be found between observed and simulated BC and CO trend with correlations of 0.62 and 0.46, respectively. Please note that CO and BC are systematic underestimated in the latter part of MTX2006, which has also been seen in other modeling studies for the coastal area of China, where the transport of high CO (>500 ppbv) from CEC was underestimated (Zhang et al., 2003). The underestimation is attributed by the uncertainties of the emission

ACPD
8, 13159–13195, 2008

databases. The work of Streets et al. (2003) reported 156% and 484% uncertainties in China's CO and BC emissions. Wang et al. (2004) indicated that the emissions of CO in 2000 have been substantially (>80%) underestimated over CEC in a bottom-up inventory by comparing model results with observations at a station in CEC and Asia Pacific rim flights. Recent work of Streets (D. G. Streets, personal communication) shows a 300% increase of industry sector in this region since 2000.

As shown in Fig. 3a, the model simulations were able to reproduce the two high pollution cases defined in Sect. 3.1. In the Case II, the simulated O_3, CO, NO_x and BC are 97 ppbv, 729 ppbv, 2.6 ppbv and 6.7μgC/m^3, respectively, close to the observed values of 98 ppbv, 734 ppbv, 2.5 ppbv and 8.2μgC/m^3. The model also produced non-observed peaks of ozone at 10:00 UTC on 13 June. This is attributed to the discrepancy of the modeled winds. From 13 June, the observed wind changed its direction from south to west or north, and brought clear air masses. However, the modeled wind remains still northward till 14 June and transported high ozone from the southern part of Mt. Tai, where a large amount of pollutants are emitted from biomass burning shown in Table 2. In Case I, the simulation underestimated the mixing ratios of pollutants, but captured the trend well. In Case I, the modeled O_3 , CO, NO_x and BC are 100 ppbv, 523 ppbv, 1.7 ppbv and 3.9μgC/m^3, lower than the observed values of 110 ppbv, 902 ppbv, 1.9 ppbv and 8.7μgC/m^3. This is caused by the coarse time and grid resolutions of the biomass burning emissions. As shown in Table 2, there are strong burning activities to the south of Mt. Tai, especially in the SSD region (only 150 km away from the observing site). The coarse resolution of 1° and 8 days of the inventory make it hard to precisely represent the inhomogeneous spatial and temporal distributions of real emissions.

The observed and modeled correlations between O_3 and its precursors (CO and NO_x) at Mt. Tai are shown in Fig. 4 to assess the model performance in the photochemical processes. We applied the Reduced Major Axis (RMA) regression method to calculate the slope, interception and correlation coefficient, rather than the standard linear least squares regression analyses since these measurements are subjected

to error. It's clear that the simulated regression line between O_3 and CO is in good agreement with the observed one. Compared with its outflow region (the North Pacific, 0.12–0.35 ppbv/ppbv), Mt. Tai shows a smaller slope of O_3 versus CO (model: 0.078 ppbv/ppbv; observation: 0.085 ppbv/ppbv) (Pochanart et al., 1999; Tanimoto et al., 2002), which might be related to the titration during the transport. The correlation between O_3 and NO_x is quite different. O_3 and NO_x generally have a positive correlation during low NO_x (2.0 ppbv), while it became negative under high NO_x (4.0 ppbv) condition. This pattern has also been well reproduced by the model.

The model simulations have further been validated with comparing the model results with concentrations of O_3 and CO observed at Yonaguni (123.02°E, 24.47°N, 30 m a.s.l) (Fig. 3b). Yonaguni is a sea-level station located in the western Pacific in the network of the World Data Centre for Greenhouse Gases (WDCGG) (http://gaw.kishou.go.jp/wdcgg/). As shown in Fig. 3b and Table 3, temporal variation of the hourly mean concentrations was reproduced satisfactorily, although CO has been underestimated.

The model is capable of well reproducing the spatial and temporal variations of the observed ozone concentrations and its precursors during the study period. It provides us with confidence in the model-derived contributions of CEC ozone from different source regions in this study.

3.2 Attribution of origins of near-ground ozone over CEC

3.2.1 Monthly mean attributions

Figure 5 illustrates modeled monthly mean O_3 concentrations (shaded) and wind fields (arrows) in the lower troposphere (below 1.5 km) in June 2006. It's clear that CEC is covered with air masses of high ozone (65–85 ppbv). Mt. Tai is located in the center of high ozone region with prevailing northward wind. In this section, we analyze the results of the simulated tagged O_3 to examine the source region of ozone, focusing on the contributions of each area and the role of regional transport.

Table 4 shows the estimated contributions of ozone mixing ratios at Mt. Tai from

selected source regions shown in Fig. 1 and Table 1. To better describe the interactions between different regions in CEC, we provide the results of each region in CEC and treat the other source regions as the outer region (Outer) (including SIB, NWCHN, SWCHN, SCHN, ECHN, NECHN, PAC, KOR, JPN, and SEASA).

In general, the photochemical production of ozone in CEC is the most important mechanism leading to a monthly mean ozone mixing ratios of 51.4 ppbv (60.2%). The ozone from photochemical productions over the other regions, lateral and top boundary is 3.1 (3.7%), 14.0 (16.4%) and 16.7 ppbv (19.6%), respectively. Table 4 indicates that the regional transport plays the major role (41.6 ppbv and 48.7%) of the high concentration of O_3 at Mt. Tai, rather than the local photochemical productions (9.8 ppbv and 11.5%), which agrees well with the work of Kanaya et al. (this issue). In their work, in situ photochemical production shows no large differences between high and low ozone cases at the station. Ozone formed in SSD, AH and JS takes the most fractions (32.4 ppbv 37.9% of total ozone). This is attributed to high emission rates in that area and favored meteorological conditions. As shown in Table 2, there are also high NO_x anthropogenic emissions over these regions. In addition, due to heavy post-harvest agricultural waste burning activities (Fu et al., 2007), a large amount of pollutants (even more than anthropogenic emissions) are emitted (Table 2) in this region. Under northwestward wind conditions (Fig. 5), high ozone formed in these regions is transported to Mt. Tai.

Figure 6 shows the horizontal distribution of monthly mean contributions to near-ground ozone from photochemical reactions in different sources regions, lateral and top conditions. As shown in Fig. 6, 25–60 ppbv (30–70%) of O_3 concentrations over CEC are from the photochemical production in this region. The highest concentration of chemically produced O_3 (55 ppbv, 60%) is to the south of Mt. Tai (Fig. 6a). The contributions from lateral and top conditions are 10–20 and 15–25 ppbv over CEC, respectively (Fig. 6e and f), and it exhibits a pattern of minimum in polluting regions-maximum in remote area. Due to the effect of regional transport, the influenced areas around an O_3 formeing source region are expanded remarkably. For example, chem-

ACPD
8, 13159–13195, 2008

ically produced ozone resulted from the south of CEC (SSD+AH+JS) is transported northeastwardly to HBT, where the contribution of transport reaches around 5–10 ppbv (5–15%) (Fig. 6c). Similarly, chemically produced ozone in Local, NSD, ESD, and HBT is transported out of CEC to the Northeast of China (Fig. 6b).

It is useful to compare the results with other studies as well (Yamaji et al., 2006; Wang et al., 1998). Our results show a little higher contribution of photochemical reactions over CEC (25–60 ppbv, 30–70%) than the estimations (15–30 ppbv and 30–60%) made by Yamaji et al. (2006) using emissions sensitive approach. The on-line tracer-tagged technology used in this study appears to give a more accurate quantification of transport due to the importance of non-linearities in the transport and fast photochemistry of ozone and its precursors, whereas the sensitivity approach provides a more policy-relevant quantification by describing responses to emission controls (Derwent et al., 2004). In the contribution from top condition, the simulated result is similar with work of Wang et al. (1998). In their study, the zone averaged contribution to near-ground ozone from upper air (>400 hpa) in July between 30°N and 40°N is 15–25%.

3.2.2 Attributions during three cases

Table 4 shows the estimation of attributions during two high pollution cases (Case I and II) and a clean case (Case III) at Mt. Tai. Fig. 7 presents the spatial distributions of contributions from different sources in the same period.

Case I: As shown in Fig. 7a, the meteorological conditions over CEC are controlled by a stable high pressure (1008 hpa) located at the East China Sea, which favors the O_3 photochemical production and northward transport. Meantime, there are strong biomass burning activities in the south of CEC (Table 2). In SSD and AH, NO_x emission rates from biomass burning even are higher than anthropogenic NO_x. As a result, high ozone formed over SSD, AH and JS are transported northward by the southern wind. At Mt. Tai, this contribution of transport reaches 52 ppbv, more than 50% of total surface ozone levels (Table 4).

Case II: Fig. 7b indicates that Mt. Tai is situated between an inverse trough, located

in the Mongolia and Northwest China, and sub-tropical high pressure. Consequently, the strong southern wind prevails over CEC. Similar to Case I, strong biomass burning emissions covers SSD, JS, and AH (Table 2). Ozone formed in SSD and JS+AH are 5–40 ppbv (5–40%) and 10–70 ppbv (10–70%) over CEC, with 28 ppbv (29%) and 32 ppbv (33%) at Mt. Tai. Even in the Bohai Sea, the sum of transported ozone from SSD, AH and JS reaches around 20 ppbv (Fig. 7b). Table 4 shows that the contribution from chemically produced ozone in the inner CEC reaches 72 ppbv at Mt. Tai, 74% of the total surface ozone concentrations, especially the transport from SSD+AH+ JS (59 ppbv, 62%).

Case III: This case happens in 8–10 June, a period between Case I and II. The observed mean ozone is only 64 ppbv, much lower than those in Case I and II. Figure 7c shows that CEC are controlled by a strong low pressure (988 hpa), moved from Mongolia (Fig. 7a). This pattern results in clean relative air mass from north mixed with polluted air from HBT to Mt. Tai (Fig. 7c). As shown in Fig. 7c, under the strong northwestern wind, ozone from lateral boundary covers a large fraction in the north of CEC. The chemically produced O_3 over HBT and NSD is also transported southward to Mt. Tai and reaches 7.5 ppbv (11%) and 8.5 ppbv (13%), respectively. Compared with the results during Case I and II, it is clear that lower chemically produced ozone (35 ppbv), mainly from north parts of CEC (HBT, NSD and Local), is the major reason of low total ozone. So it can be concluded that the transport of strong photochemical productions from high anthropogenic and biomass burning emissions in the southern parts of CEC (SSD, AH and JS) plays a key role in high ozone events at Mt. Tai.

We have demonstrated that O_3 concentrations over CEC are controlled by the photochemical productions, and the regional transport from different source regions inner CEC, especially the southern parts (SSD, AH and JS), plays the important role in the monthly mean O_3 distributions and high ozone events. This transport from CEC southern parts even becomes the dominated mechanism at Mt. Tai.

4 Exports from CEC near-ground ozone

Figure 8 presents the spatial distributions of chemically produced ozone in CEC. Also shown are contributions from China, NECHN and ECHN in June, 2006. These regions have already been defined in Sect. 2 and Fig. 1. Here, we divide CEC into two parts by the underlyingsurface (land and ocean): CEC* (a high polluting region including HBT, SX, HN, NSD, ESD, Local, SSD, AH and JS) and CHNSEA (a clean region with no emissions, Fig. 1). In CHNSEA, most of ozone precursors are originated from the transport of CEC*, so it is treated to represent the effect on ozone mixing ratios due to the outflow of CEC* ozone precursors, while CEC* represents the outflow of chemically produced ozone itself in the high polluting region.

As shown in Fig. 8b and c, due to the prevailed southerly and southwesterly summer monsoon over CEC, O_3 formed in CEC* and CHMSEA is transported toward the northeast to Korea and Japan, where the contribution of transport to monthly mean ozone reaches 5–15 ppbv. Specially, Fig. 8b and c show that CHNSEA and CEC* cover the similar fraction over China Sea, Korea Peninsula and Japan. This indicates that the outflow of ozone precursors exerts a comparable effect on ozone with ozone itself in the export of CEC pollutants in June.

Compared with other source regions in China (Fig. 8d and e), CEC shows the most importance in the export of China pollutants (Fig. 8a). For example, the ozone export from ECHN is limited near China coasts. Similarly, the contribution from NECHN is much below 5% in Japan.

By using back trajectories analysis, Pochanart et al. (2004) estimated the regional photochemical O_3 build up due to CEC anthropogenic emissions at Oki (36.28°N, 133.18°E, 90 m a.s.l) and Happo (36.68°N, 137.8°E, 1840 m a.s.l), two remote sites in Japan, based on two-year continuous observations in 1990s. In their work, the mean photochemical buildup from CEC in air masses traveling over CEC is about 15–20 ppbv in June. Considering the fraction of this group in total air masses (about 35%), the monthly mean contribution from CEC is 5–7 ppbv, which is similar to the result

ACPD
8, 13159–13195, 2008

reported in this study and confirmed our tagged-tracer approach.

5 Summary

In this study, we applied the Nested Air Quality Prediction Model System (NAQPMS), a 3-D regional chemical transport model with an on-line tracer tagging module to investigate the sources of high ozone levels at Mt. Tai during the MTX2006 conducted by FRCGC/JAMSTEC and IAP in June 2006. The influence of various source regions has been quantitatively evaluated. The outflows of CEC ozone and its precursors are discussed. The major findings are summarized as follows.

The performance of the applied regional model has been assessed by comparing the simulated results and observations of O_3, CO, NO_x and BC. Comparisons show that the model is capable of reproducing the temporal variations of the observed ozone and other pollutants over the study period. Except a certain underestimation in Case I, the model can also capture high polluted and clean cases well.

The simulated tagged tracer, which is expected to eliminate the errors of emission sensitivity approach due to non-linearities in the transport and fast photochemistry of ozone and precursors, indicates that the regional transport from chemically produced ozone over other regions inner CEC contributes to the most fraction (49%) of near-ground mean ozone at Mt. Tai in June, rather than in-situ photochemistry (12%). In the transported chemically produced ozone, the contribution from southern parts in CEC (SSD+AH+JS) plays the most important role (32.4 ppbv, 37.9% of total ozone). The contributions from lateral and top boundaries are 16.4% (14.0 ppbv) and 19.6% (16.7 ppbv).

Model simulations of three cases also prove that the transport of strong photochemical productions from high anthropogenic and biomass burning emissions in the southern parts of CEC (SSD, AH and JS) plays a key role in high ozone events at Mt. Tai. Due to high pressure located in China East Sea or the interaction between Mongolia inverse trough sub-tropical high pressure, the southern air flows transport high ozone

ACPD
8, 13159–13195, 2008

in SSD, AH and JS to Mt. Tai. Their contributions reach 52 ppbv (52%) and 59 ppbv (62%) in Case I and II. On the contrary, the low chemically produced ozone from CEC northern parts in Case III results in the decrease of total ozone.

The month mean horizontal distributions of chemically produced ozone from various source regions indicate that O_3 concentrations over CEC are controlled by the photochemical productions and regional-scale transport plays an important role in the distribution of ozone. Chemically produced ozone resulted from the south of CEC (SSD+AH+JS) can be transported northeastwardly to northern rim of CEC (a distance of more than 800 km), where the mean contribution is 5–10 ppbv. During high ozone events, this contribution can reach 25 ppbv. Ozone produced in CEC northern parts can be transported out of CEC to Northeast China.

The outflows of CEC ozone and its precursors are investigated in the simulation. The contribution from CEC to mean ozone mixing ratios over Korea Peninsula and Japan is 5–15 ppbv in June. Specially, the chemical evolution of ozone precursors during the outflow exerts a comparable effect with direct transport of ozone itself from CEC in June.

Finally, these results are helpful to understand the sources and evolution of CEC high ozone levels, especially the role of transport. Further work is needed to further understand the seasonal cycles, which is being performed and will be the subject to a future paper.

Acknowledgements. Work of IAP in this research was funded by the Chinese Academy of Sciences (KZCX2-YW-205), the National Basic Research 973 Grant (2005CB422205) and NSFC grant (40775077). Work of JAMSTEC was sponsored by the RR2002 grant (MEXT, Japan) and the Global Environmental Research Fund, B051 (The Ministry of the Environment, Japan). The authors would like to thank all the participants in the MTX2006 field campaign. We also thank Q. Wu for GIS support, R. A. Zaveri for the CBM-Z source code, and Japan Meteorological Agency for O_3 and CO observations at Yonaguni, Japan. We gratefully acknowledge the anonymous reviewers and Y. Zhang at the Princeton University for their helpful comments and suggestions.

References

Akimoto, H., Ohara, T., Kurokawa, J., and Horii, N.: Verification of energy consumption in China during 1996–2003 by using satellite observational data, Atmos. Environ., 40, 7663–7667, 2006.

Brasseur, G., Orlannd, J. J., and Tyndal, G. S.: Atmospheric chemistry and global change, Oxford University Press, New York, USA, 1999.

Cao, G., Zhang, X., Wang, D., and Zheng, F.: Inventory of atmospheric pollutants discharged from biomass burning in China continent (in Chinese), China Environmental Science, 25(4), 389–393, 2005.

Cheung, V. and Wang, T.: Observational study of ozone pollution at a rural site in the Yangtze Delta of China, Atmos. Environ., 35, 4947–4958, 2001

Crutzen, P. J. and Lawrence, M. G., Poschl, U.: On the background photochemistry of tropospheric ozone, Tellus B, 51A, 126–146, 1999.

Davis, D. D., Chen, G., Grawford, J. H., Liu, S., Tan, D., Sandholm, S. T., Jiang, P., Cunnold, D. M., Dinunno, B., Browell, E. V., Grant, W. B., Fenn, M. A., Anerson, B. E., Barrick, J. D., Sachse, G. W., Vay, S. A., Hudgins, H., Avery, M. A., Lefer., B., Shetter, R. E., Heikes, B. G., Blake, D. R., Kondo., Y., and Oltmans, S.: An assessment of western North Pacific ozone photochemistry based on spring obsevations from NASA's PEM-West B (1994) and TRACE-P (2001) field studies, J. Geophys. Res., 108(D21), 8829, doi:10.1029/2002JD003-232, 2003.

Derwent, R. G., Stevenson, D. S., Collins, W. J., and Johnson, C. E.: Intercontinental transport and the origins of the ozone observed at surface sites in Europe, Atmos. Environ., 38, 1891–1901, 2004.

Ding, A., Wang, T., Thouret, V., Cammas, J.-P., and Nédélec, P.: Tropospheric ozone climatology over Beijing: analysis of aircraft data from the MOZAIC program, Atmos. Chem. Phys., 8, 1–13, 2008, http://www.atmos-chem-phys.net/8/1/2008/.

Fu, T. M., Jacob, D. J., Palmer, P. I., Chance, K., Wang, Y. X., Barletta, B., Balke, D. R., Stanton, J. C., and Pilling, M.: Space-based formaldehyde measurements as constraints on volatile organic compound emissions in east and south Asia and implications for ozone, J. Geophys. Res., 112, D06312, doi:10.1029/2006JD007853, 2007.

Gao, J., Wang, T., Ding, A., and Liu, C.: Observational study of ozone and carbon monoxide

ACPD

8, 13159–13195, 2008

at the summit of mount Tai (1534 m a.s.l.) in central-eastern China, Atmos. Environ., 39, 4779–4791, 2005.
Giglio L., Descloitres J., Justice, C. O., and Kaufman, Y. J.: An enhanced contextual fire detection algorithm for MODIS, Remote Sens. Environ, 87(2–3), 273–282, 2003.
Grell, G. A., Dudhia, J., and Stauffer, D. R.: A description of the Fifth-Generation Penn State/NCAR Mesoscale Model (MM5), Technical Note: NCAR/TN-398+STR, Natl. Cent. For Atmos. Res., Boulder, CO, USA, 122 pp., 1994.
Guenther, A., Hewitt, C. N., Erickson, D., Fall, R., Geron, C., Graedel, T., Harley, P., Klinger, L., Lerdau, M., McKay, W. A., Scholes, B., Steinbrecher, R., Tallamraju, R., Taylor, J., and Zimmerman, P.: A global model of natural volatile organic compound emissions, J. Geophys. Res., 100(D5), 8873–8892, 1995.
He, Y., Uno, I., Wang, Z., Ohara, T., Sugimoto, N., Shimizu, A., Richter, and A., Burrows, J.: Variations of the increasing trend of tropospheric NO_2 over central east China during the past decade, Atmos. Environ., 41, 4865–4876, 2007.
Intergovernmental Panel on Climate Change (IPCC): Climate Change 1995: the Science of Climate Change, edited by: Houghton, J. T., Ding, Y., Griggs, D. J., Noguer, M., van der Linden, P. J., Dai, X., Maskell, K., and Johnson, C. A., Cambridge Univ. Press, New York, USA, 1996.
Kondo, Y., Nakamyra, K., Chen, G., Takega, N., Koike, M., Miyazaki, Y., Kita, K., Crawford, J., Ko, M., Kawakami, S., Shirai, T., Liley, Wang, Y., and Ogawa, T.: Photochemistry of ozone over western Pacific from winter to spring, J. Geophys. Res., 109, D23S02, doi:10.1029/2004JD004871, 2004.
Li, J., Wang, Z., Akimoto, H., Gao, C., Pochanart, P., and Wang, X.: Modeling study of ozone seasonal cycle in lower troposphere over East Asia, J. Geophys. Res., 112, D22S25, doi:10.1029/2006JD008209, 2007.
Liu, H., Jacob, D., Bey, I., Yantosca, R. M., and Duncan, B.: Transport pathways for Asian pollution outflow over the Pacific: Interannual and seasonal variations, J. Geophys. Res., 108(D20), 8786, doi:10.1029/2002-JD003102, 2003.
Liu, H., Jacob, D., Bey, I., Yantosca, R. M., and Duncan, B.: Transport pathways for Asian pollution outflow over the Pacific: Interannual and seasonal variations, J. Geophys. Res., 108(D20), 8786, doi:10.1029/2002-JD003102, 2003.
Naja, M., Akimoto, H.: Contribution of regional pollution and long-range transport to the Asia-Pacific region: Analysis of long-term ozonesonde data over Japan, J. Geophys. Res.,

109(D2), D21306, doi:10.1029/2004JD004687, 2004.
Ohara, T., Akimoto, H., Kurokawa, J., Horii, N., Yamaji, K., Yan, X., and Hayasaka, T.: An Asian emission inventory of anthropogenic emission sources for the period 19802020, Atmos. Chem. Phys., 7, 4419–4444, 2007, http://www.atmos-chem-phys.net/7/4419/2007/.
Pochanart, P., Hirokawa, J., Kajii, Y., and Akimoto, H.: Influence of regional-scale anthropogenic activity in northeast Asia on seasonal variations of surface ozone and carbon monoxide observed at Oki, Japan, J. Geophys. Res., 109(D3), 3621–3631, 1999.
Pochanart, P., Kato, N., Katsuno, T., and Akimoto, H.: Eurasian continental background and regionally polluted levels of ozone and CO observed in northeast Asia, Atmos. Environ., 38, 1325–1336, 2004.
Richter, A., Burrows, J. P., Nüß, H., Granier, C., and Niemeier, U.: Increase in tropospheric nitrogen dioxide over China observed from space, Nature, 437, 129–132, 2005.
Streets, D. G., Bond, T. C., Carmichael, G. R., Fernandes, S. D., Fu, Q., He, D., Klimont, Z., Nelson, S. M., Tsai, N. Y., Wang, M. Q., Woo, J. H., and Yarber, K. F.: An inventory of gaseous and primary aerosol emissions in Asia in the year 2000, J. Geophys. Res., 108(D21), 8809, doi:10.1029/2002JD003093, 2003.
Streets, D. G. and Waldhoff, S. T.: Present and future emissions of air pollutants in China: SO_2, NO_x, and CO, Atmos. Environ., 34, 363–374, 2000.
Sudo, K. and Akimoto, H.: Global source attribution of tropospheric ozone: long-range transport from various source regions, J. Geophys. Res., 112, D12302, doi:10.1029/2006JD007992, 2007.
Sudo, K., Takahashi, M., Kurokawa, J., Akimoto, H.: Chaser: A global chemical model of the troposphere, 1: model description, J. Geophys. Res., 107(D17), 4339, doi:10.1029/2001JD001113, 2002.
Tanimoto H., Wild, O., Kato, S., Furutani, H., Makide, Y., Komazaki, Y., Hashimoto, S., Tanaka, S., and Akimoto, H.: Seasonal cycles of ozone and oxidized nitrogen species in northeast Asia, 2: a model analysis of the roles of chemistry and transport, J. Geophys. Res., 107(D23), 4706, doi:10.1029/2001JD001497, 2002.
Van der Werf, G. R., Randerson, J. T., Giglio, L., Collatz, G. J., and Kasibhatla, P. S.: Interannual variability in global biomass burning emission from 1997 to 2004, Atmos. Chem. Phys., 6, 3423–3441, 2006, http://www.atmos-chem-phys.net/6/3423/2006/.

Waleck, C. J. and Aleksic, N. M.: A simple but accurate mass conservative peak-preserving, mixing ratio bounded advection algorithm with Fortran code, Atmos. Environ., 32, 3863–3880, 1998.

Wang, T., Ding, A., Gao, J., and Wu, W.: Strong ozone production in urban plumes from Beijing, China, Geophys. Res. Lett., 33, L21806, doi:10.1029/2006-GL027689, 2006a.

Wang, T., Vincent, T. F., Cheung, M. A., and Li, Y. S.: Ozone and related gaseous pollutants in the boundary layer of eastern China: overview of the recent measurements at a rural site, Geophys. Res. Lett., 28, 2373–2376, 2001a.

Wang, Y., Jacob, D., and Logan, J.: Global simulation of tropospheric O_3-NO_x-hydrocarbon chemistry, 3: origin of tropospheric ozone and effects of nonmethane hydrocarbons, J. Geophys. Res., 103(D9), 10 757–10 768, 1998.

Wang, Y., McElroy, M. B., Wang, T., and Palmer, P.: Asian emissions of CO and NO_x constraints from aircraft and Chinese station data, J. Geophys. Res., 109, D24304, doi:610.1029/2004JD005250, 2004.

Wang, Z., Akimoto, H., and Uno, I.: Neutralization of soil aerosol and its impact on the distribution of acid rain over East Asia: observations and model results, J. Geophys. Res., 107(D19), 4389, doi:10.1029/2001JD-001040, 2002.

Wang, Z., Huang, M., He, D., Xu, H., and Zhou, L.: Sulfur distribution and transport studies in East Asia using Eulerian model, Advance of Atmospheric Science, 13, 399–409, 1996.

Wang, Z., Li, J., Wang, X., Pochanart, P., and Akimoto, H.: Modeling of regional high ozone episode observed at two mountain sites (Mt. Tai and Huang) in East China, J. Atmos. Chem., 55(3), 253–272, 2006b.

Wang Z., Maeda, T., Hayashi, M., Hsiao, L. F., and Liu, K. Y.: A nested air quality prediction modeling system for urban and regional scales, application for high-ozone episode in Taiwan, Water, Air, and Soil Pollut., 130, 391–396, 2001b.

Wang Z., Ueda, H., and Huang, M.: A deflation module for use in modeling long-range transport of yellow sand over East Asia, J. Geophys. Res., 104, 26 947–26 960, 2000.

Wesely, M. L.: Parameterization of surface resistances to gaseous dry deposition in regional-scale numerical models, Atmos. Environ., 23, 1293–1304, 1989.

Xu, X., Lin, W., Wang, T., Yan, P., Tang, J., Meng, Z., and Wang, Y.: Long-term trend of surface ozone at a regional background station in eastern China 19912006: enhanced variability, Atmos. Chem. Phys., 8, 2595–2607, 2008, http://www.atmos-chem-phys.net/8/2595/2008/.

Yamaji, K., Ohara, T., Uno, I., Tanimoto, H., Kurokawa, J., and Akimoto, H.: Analysis of the seasonal variation of ozone in the boundary layer in East Asia using the Community Multi-scale Air Quality model: what controls surface ozone levels over Japan?, Atmos. Environ., 40, 1856–1868, 2006.

Zaveri, R. A. and Peters, L. K.: A new lumped structure photochemical mechanism for large-scale applications, J. Geophys. Res., 104, 30 387–30 415, 1999.

Zhang, M., Uno, I., Carmichael, G. R, Akimoto, H., Wang, Z. F., Tang, Y. H., Woo, J. H., Streets, D. J., Sachse, G.W., Avery, M. A., Weber, R. J., and Talbot, R. W.: Large-scale structure of trace gas and aerosol distributions over the western Pacific Ocean during the Transport and Chemical Evolution Over the Pacific (TRACE-P) experiment, J. Geophys. Res., 108(D21), 8820, doi:610.1029/2002JD002946, 2003.

Zhu, B., Akimoto, H., Wang, Z., Sudo, K., Tang, J., and Uno, I.: Why does surface ozone peak in summertime at Waliguan?, Geophys. Res. Lett., 31, L17104, doi:10.1029/2004GL020609, 2004.

Table 1. Tagged source regions in East Asia.

Regions[a]	Description
Local	Tai'an and Lai'wu city, ShanDong province, China
SSD	Southern ShanDong province, China
ESD	Eastern ShanDong province, China
NSD	Northern ShanDong province, China
HBT	Hebei, Beijing, and Tianjin, China
SX	ShanXi province, China
HN	HeNan province, China
AH	AnHui province, China
JS	JiangSu province, China
CHNSEA	CHiNa SEA, incl. Bohai Sea, Huanghai Sea and East Sea
NECHN	NorthEast CHiNa, incl. Heilongjiang, Jilin and Liaoning provinces, China
ECHN	East CHiNa, incl. Shanghai, Zhejiang, Fujian, Jiangxi and Taiwan provinces, China
SCHN	South CHiNa, incl. Hubei, Hunan, Guangdong, Guangxi, Hainan and HongKong provinces, China
SWCHN	SouthWest CHiNa, incl. Sichuan, Chongqing, Guizhou, Yunnan, and Tibet provinces, China
NWCHN	NorthWest CHiNa, incl. Shanxi, Gansu, Qinghai, Ningxia, Xinjiang, and Neimenggu provinces, China
KOR	KORea
JPN	JaPaN
SIB	SIBeria
PAC	western PACific rim
SEASA	SouthEast ASiA

ACPD
8, 13159–13195, 2008

Table 2. Model NO_x emissions in Ton NO_2/month from the major sources regions over CEC.

Regions[a]	Anthropogenic[b]	BB[c]	BB1[c]	BB2[c]	BB3[c]	BB4[c]	Area[d]
Local	8659	3623	876	1665	1025	57	1.0
SSD	20633	55525	13508	37697	3006	1314	5.1
ESD	18833	21845	5052	10230	3970	2593	6.9
NSD	16772	6837	1214	1661	3929	33	2.7
HBT	126810	16269	261	5089	9127	1892	21.8
SX	59131	5586	1143	1830	1809	804	15.6
HN	69522	52279	33243	15042	3841	153	16.7
AH	51021	54465	20728	33065	530	142	13.9
JS	97156	77279	12268	62355	2567	89	10.3
CHNSEA	0	0	0	0	0	0	0
Total	468537	293708	85493	164634	25804	5319	94

[a] Region names are shown in Fig. 1.

[b] Anthropogenic emissions incl. fossifuel, biofuel, industrial excl. open biomass burning.

[c] BB is the monthly emissions from Biomass burning in Ton NO_2/mon. BB1, BB2, BB3, and BB4 represent the emissions during 2–9, 10–17, 18–25, and 26–30 June from biomass burning. Units are Ton NO_2/8 days.

[d] Unit is 10^5 km^2.

ACPD
8, 13159–13195, 2008

Table 3. Statistical summary of comparisons of the model results with observations.[a]

	N[b]	C_{mod}[c]	C_{obs}[c]	NB	RMSE	R
Mt. Tai						
O_3	666 (28)	85	82	3.7 (4.0)	22.3 (14.2)	0.56 (0.69)
CO	641 (28)	417	560	−125.1 (-120.5)	378.6 (265.8)	0.25(0.46)
NO_x	681 (28)	1.2	1.1	0.1 (0.1)	1.2 (0.6)	0.30 (0.62)
BC	720 (28)	2.7	3.4	−0.6 (0.6)	3.4 (2.3)	0.41 (0.62)
Yonaguni						
O_3	719 (30)	24	24	1.1 (0.7)	11.2 (9.0)	0.82 (0.93)
CO	703 (30)	75	112	−38.1 (−43.9)	57.9 (55)	0.81 (0.87)

[a] Values in bracket denote daily mean concentrations. Others are hourly mean concentrations. Units are ppbv except for BC which is $\mu gC/m^3$.

[b] N is the number of observed samples. For model results, N is 720 h and 30 days.

[c] C_{mod} and C_{obs} represent the modeled (all hours) and observed mean concentrations (lacked hours are omitted).

ACPD
8, 13159–13195, 2008

Table 4. Contributions to ozone mixing ratios at Mt. Tai from selected source regions.[a]

Regions	Monthly mean	Case I	Case II	Case III
Local	9.8 (11.5)	9.3 (9.3)	7 .0 (7.2)	12 .1 (18.3)
ESD	1 (1.2)	0.1 (0.1)	0 (0)	0 (0)
SSD	18.5 (21.5)	29.8 (29.8)	27.6 (28.5)	2.9 (4.2)
NSD	2 .2 (2.6)	0.1 (0.1)	0 (0.1)	8.5 (12.9)
HBT	1.5 (1.8)	0.2 (0.2)	0.5 (0.5)	7.5 (11.3)
SX	0.4 (0.5)	0.1 (0.1)	0.6 (0.6)	1.2 (1.8)
HN	2.8 (3.3)	1.0 (1.0)	3.6 (3.7)	1.1 (1.6)
AH	5.6 (6.6)	6.6 (6.6)	12.8 (13.2)	0.7 (1.1)
JS	8.3 (9.8)	14.8 (14.8)	18.8 (19.4)	1.0 (1.6)
CHNSEA	1.3 (1.5)	1.0 (1.0)	0.7 (0.7)	0.1 (0.2)
Inner[b]	51.4 (60.2)	63.1 (63.1)	71.7 (73.8)	35.2 (53.0)
Outer[b]	3.1 (3.7)	3.0 (3.0)	2.4 (2.5)	1.6 (2.5)
Boundary[c]	14.0 (16.4)	12.2 (12.1)	11.9 (12.2)	19.9 (30.0)
Upper[c]	16.7 (19.6)	21.8 (21.8)	11.1 (11.4)	9.6 (14.5)
Total	85.4 (100)	100.1 (100)	97.2 (100)	66.3 (100)

[a] Units are ppbv with percentages indicated in brackets.

[b] Inner is the sum of 10 source regions in CEC, and outer is the sum of the other regions.

[c] Boundary and Upper represent the contributions from lateral and top boundary conditions.

ACPD

8, 13159–13195, 2008

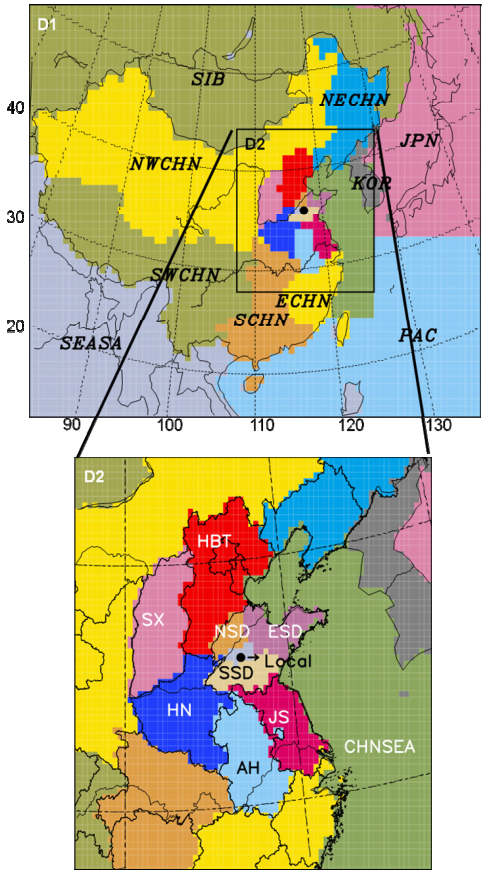

Fig. 1. Two nested model domain for NAQPMS used in this study. Also shown are regional separations for tracer tagging (characters). The marked solid cycle represents the location of Mt. Tai. CEC consists of Local, SSD, ESD, NSD, HBT, SX, HN, AH , JS and CHNSEA.

ACPD
8, 13159–13195, 2008

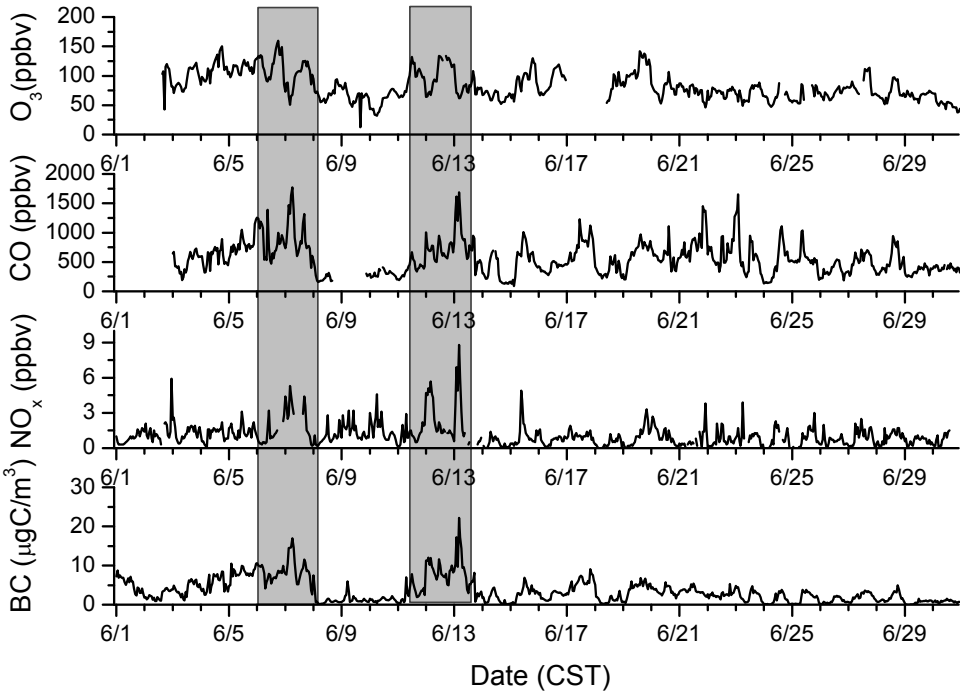

Fig. 2. Observed hourly averaged O_3, CO, NO_x and BC at Mt. Tai in June 2006. Two heavy pollution cases are marked by the semi-transparent shaded.

ACPD

8, 13159–13195, 2008

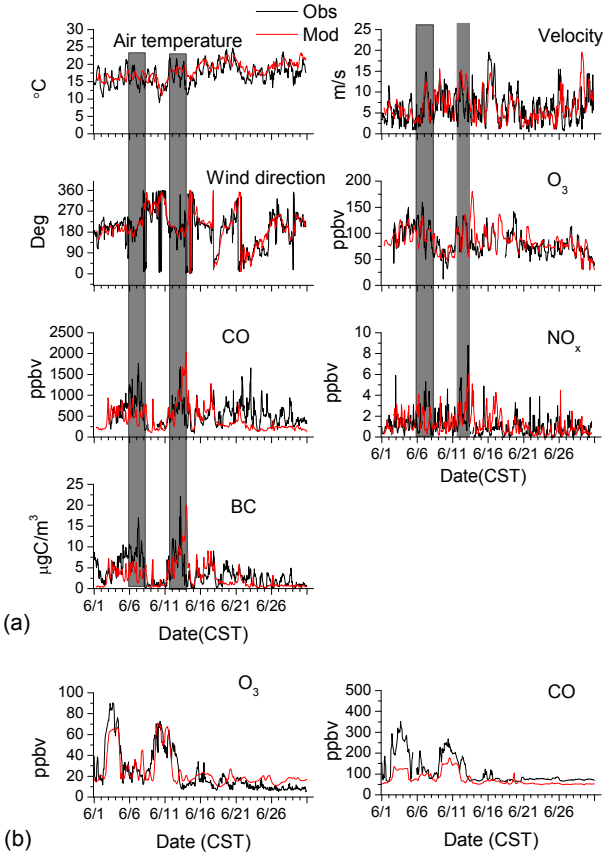

Fig. 3. Time profile of the model predicted and observed meteorological and chemical parameters during June 2006 at **(a)** Mt. Tai, **(b)** Yonaguni (123.02°E, 24.47°N, 30 m a.s.l). The semi-transparent shade represents high pollution episodes.

ACPD
8, 13159–13195, 2008

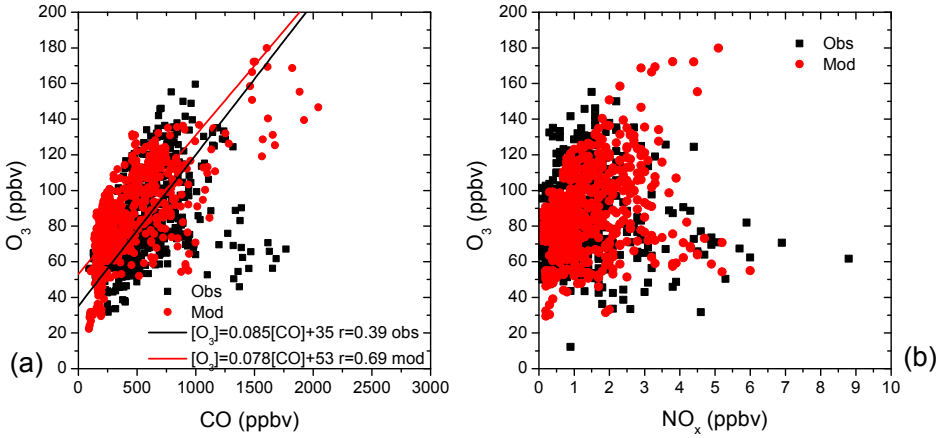

Fig. 4. Scatter plots of O_3 vs. **(a)** CO and **(b)** NO_x observed (solid squares) and predicted by the model (solid cycles) at Mt. Tai in June, 2006. The regression statistics are determined by the reduced major axis method.

ACPD
8, 13159–13195, 2008

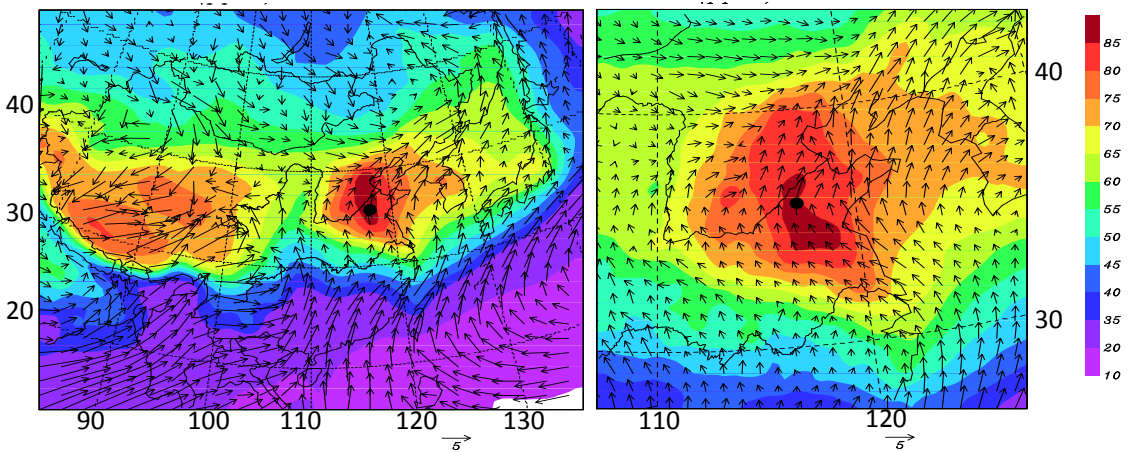

Fig. 5. Simulated monthly mean near-ground (<1.5km) ozone (ppbv, shaded) and wind vector (m/s, arrows) in June 2006 in two domains (Left: Domain 1; Right: Domain 2). Mt. Tai is marked by the dark solid cycles.

ACPD

8, 13159–13195, 2008

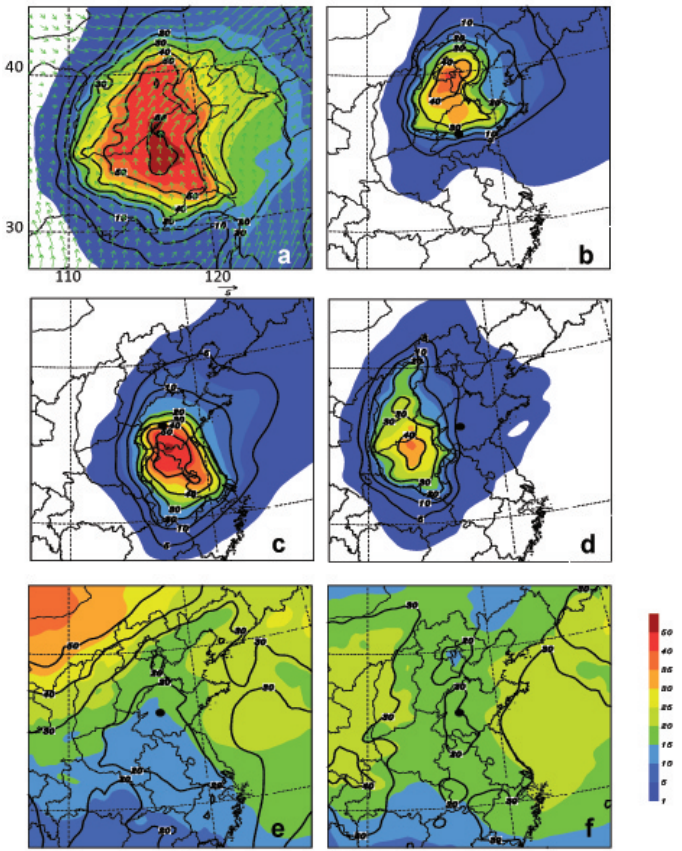

Fig. 6. Spatial distributions of contributions (shaded: ppbv; contours: %) to monthly mean near-ground (<1.5 km) ozone in June in CEC from **(a)** all photochemical production inner CEC, **(b)** HBT+NSD+ESD+Local, **(c)** SSD+AH+JS, **(d)** SX+HN, **(e)** Lateral boundary, and **(f)** top boundary. Mt. Tai is marked by the dark solid cycles.

ACPD
8, 13159–13195, 2008

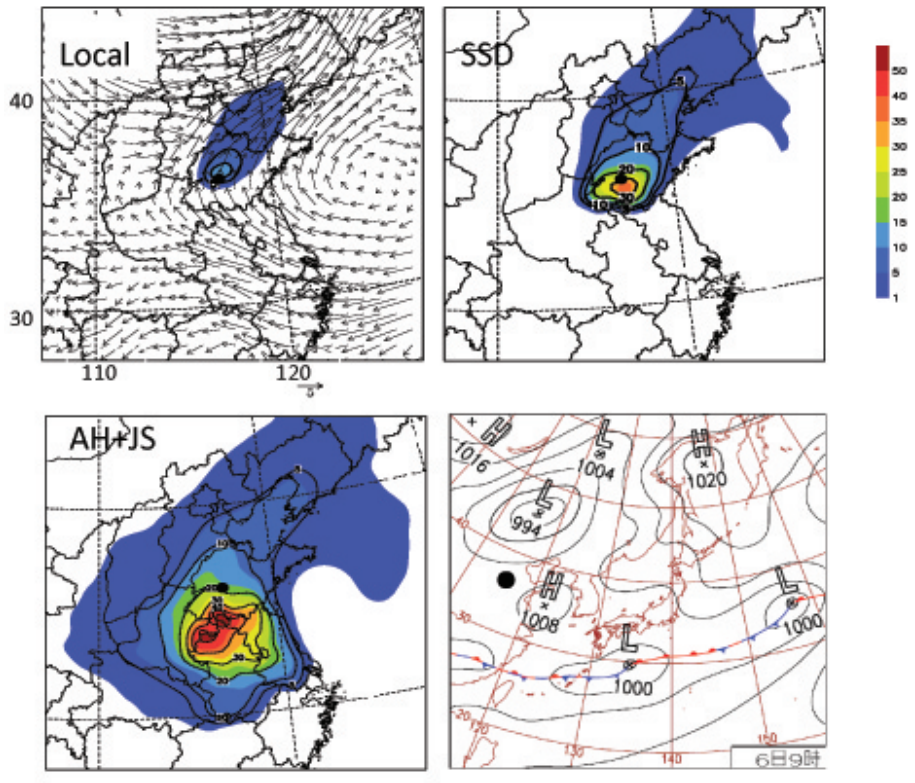

Fig. 7a. Spatial distributions of contributions (shaded: ppbv; contours: %) to near-ground (<1.5 km) ozone in Case I from **(a)** Local, **(b)** SSD, and **(c)** AH+JS. The surface weather chart at 09Z06June 2006 is also shown from Japan Meteorological Agency (http://www.data.jma.go.jp/fcd/yoho/hibiten/index.html).

ACPD
8, 13159–13195, 2008

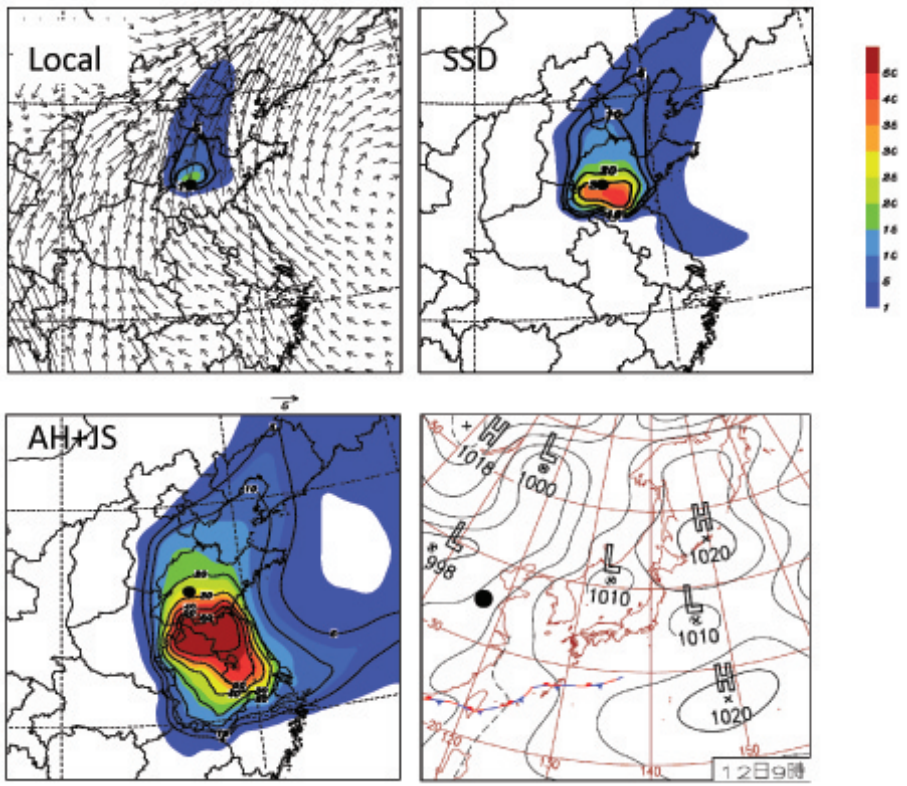

Fig. 7b. Same as Fig. 7a, but in Case II.

ACPD
8, 13159–13195, 2008

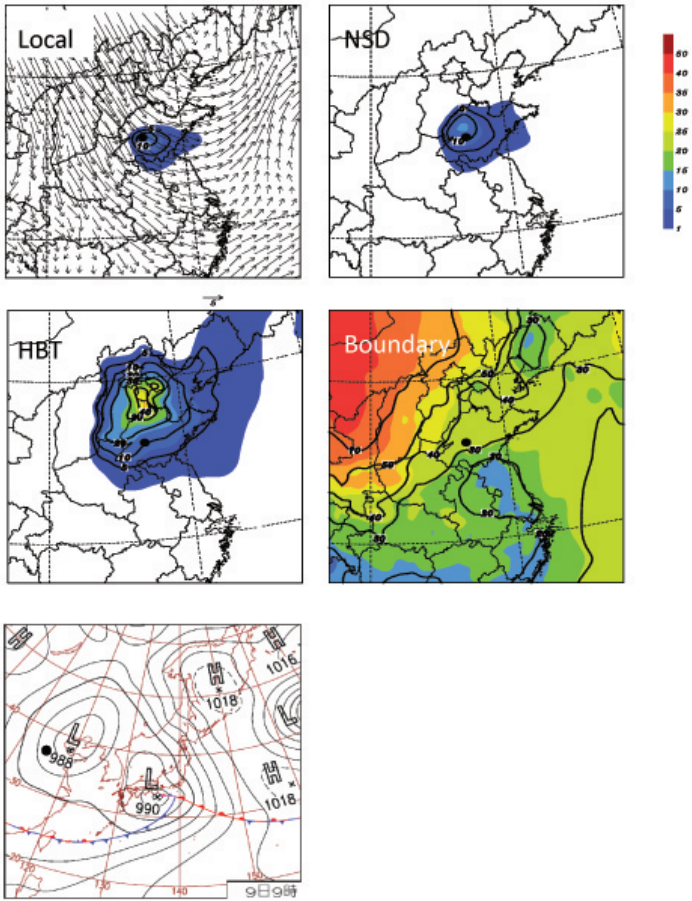

Fig. 7c. Same as Fig. 7a, but in Case III. The sources are: Local, NSD, HBT and Lateral Boundary.

ACPD
8, 13159–13195, 2008

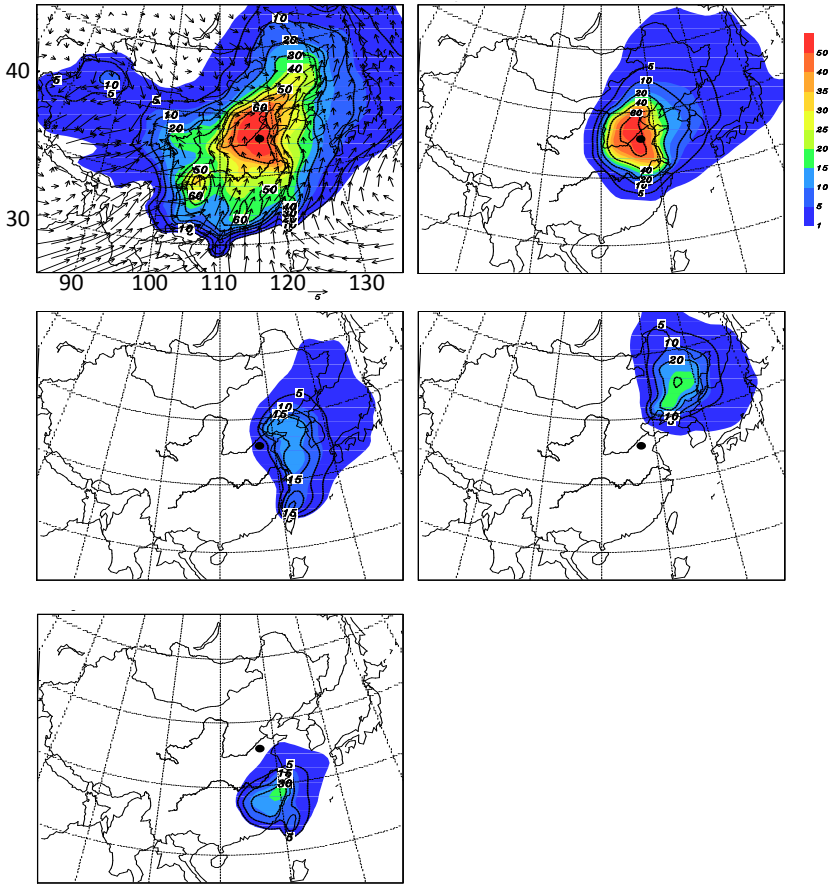

Fig. 8. Distributions of contributions (shaded: ppbv; contours: %) from chemically produced ozone over **(a)** China, **(b)** CEC*, **(c)** CHNSEA, **(d)** NECHN and **(e)** ECHN in June 2006. Also shown is wind filed in (a).

ACPD
8, 13159–13195, 2008